ACS APPLIED MATERIALS & INTERFACES

Research Article

www.acsami.org

Structural Insights into Magnetic Clusters Grown Inside Virus Capsids

M. Jaafar,[†,‡,¶] A. A. A. Aljabali,[⊥,⊗,¶] I. Berlanga,[§] R. Mas-Ballesté,[§] P. Saxena,[⊥,▽] S. Warren,[∥] G. P. Lomonossoff,[⊥] D. J. Evans,[#] and P. J. de Pablo*[,†]

[†]Departamento de Física de la Materia Condensada y Condensed Matter Physics Center (IFIMAC), Universidad Autónoma de Madrid, 28049 Madrid, Spain

[‡]Instituto de Ciencia de Materiales de Madrid, CSIC, 28049 Madrid, Spain

[§]Departamento de Química Inórgánica, Universidad Autónoma de Madrid, 28049 Madrid, Spain

[⊥]Department of Biological Chemistry, John Innes Centre, Norwich Research Park, Norwich NR4 7UH, United Kingdom

[∥]Department of Materials, University of Oxford, Begbroke Science Park, Woodstock Road Oxford OX5 1PF, United Kingdom

[#]Department of Chemistry, University of Hull, Hull HU6 7RX, United Kingdom

Supporting Information

ABSTRACT: Magnetic nanoparticles have multiple applications in materials science. In particular, virus capsids have been suggested as promising templates for building up nanometric-sized magnetic clusters by taking advantage of their inner cavity as a nanoreactor. In this study we investigate the magnetization of individual cobalt-filled cowpea mosaic virus empty virus-like particles using atomic force microscopy. We also combine the analysis of the effects of dehydration on the structure of virus particles with a comparison of their magnetic signal to that provided by commercially available magnetic nanoparticles of similar size. These two approaches allow the evaluation of the structure of the metallic cluster grown inside the virus capsid. We conclude that, rather than forming solid clusters, cobalt inside viruses forms a discontinuous structure that does not completely fill the virus cavity and reaches about 10% of its volume.

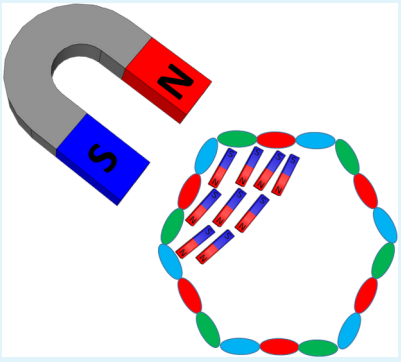

KEYWORDS: *magnetic nanoparticles, nanoreactors, protein cages, virus capsid, magnetic force microscopy*

INTRODUCTION

Virus capsids, and other protein cages, are increasingly being used as multifunctional nanocontainers for applications in materials synthesis, drug encapsulation and delivery, and catalysis.[1−7] Virus-like particles (VLPs) resemble viruses but are noninfectious, as they lack the viral genetic material. Their monodispersity, morphological and structural uniformity, biocompatibility, safety, amenability to chemical and genetic modifications, and their stability over a wide range of conditions makes them ideal nanocontainers. Cowpea mosaic virus (CPMV) empty VLPs (eVLPs) can be produced in large quantities in plants using an expression system known as pEAQ vector.[8,9] Previously, we have reported the loading of the CPMV eVLPs with cobalt and iron oxide.[10] To move closer toward the development of CPMV eVLPs for such applications as magnetic hyperthermia treatments,[11,12] it is essential to investigate the magnetic moment of individual particles because they are required to be easily manipulated by magnetic fields. Their magnetic properties are related, in turn, with the amount of metal accumulated in the eVLP cavity.

The cavity of icosahedral virus capsid architectures is an ideal size-constrained environment where the interior surface can direct the nucleation of nanomaterials. In particular, the positively charged interior surface of cowpea chlorotic mottle virus (CCMV), which has an interior cavity diameter of approximately 24 nm, has been used for directing mineralization reactions to form spatially constrained nanoparticles such as β-TiO_2.[5] In addition, the interior surface of the CCMV capsid can be altered to change its charge from positive to negative, thereby allowing the mineral nucleation of transition metal oxides such as γ-FeO(OH).[2] This internal mineralization takes advantage of the interaction between cationic ions and the inner cavity of the virus particles, which acts as a nucleation surface for metal formation. Besides, the virus capsid does not require any further modification. In other words, a gradual growth of the nanoparticle occurs simultaneously to the entry of the precursors within the inner cavity of the virus particles. This approach results in completely filled virus capsids.[2]

Recently, the related virus CPMV has been developed extensively as a template for external mineralization, to produce narrowly disperse metallic nanoparticles, and CPMV eVLP for metallo-nanoparticle growth within the cavity.[4,10] CPMV and CPMV eVLPs can be readily isolated from plants in high yields. Metallic nanoparticles can be grown inside CPMV eVLPs capsids by incubation with a solution containing a metal salt and, once the precursor is inside the virus, adding a reducing

Received: August 22, 2014
Accepted: November 18, 2014
Published: November 18, 2014

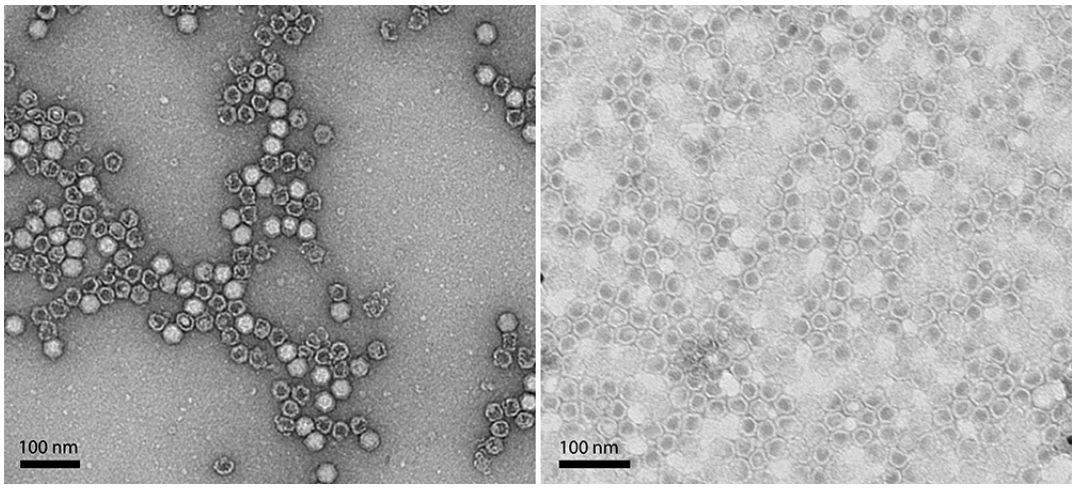

Figure 1. TEM images of CPMV particles. Left, 2% uranyl acetate stained particles of CPMV eVLPs and right, unstained Co-VLPs showing the cobalt as a core and a white ring around it representing the virus coat protein.

agent that induces the deposition of metal within the capsid.[10] In this case, the virus is used as a nanoreactor and the deposition reaction is not started until the virus is completely loaded with the corresponding precursor. Specifically, this procedure has used cobalt chloride as the metal precursor and sodium borohydride as a reducing agent. Electron microscopy (EM) imaging provides a comparison between eVLPs and loaded viruses (Co-VLPs) by the different contrast inside the particles; unmodified particles were invisible under transmission electron microscopy (TEM).[10] The TEM data suggested that the virus cages are completely filled with metallic cobalt (Figure 1).

These observations inform us about the presence of metal inside the virus but not about its structure. However, current chemical understanding of such systems indicates that one incubation cycle does not necessarily result in a high enough concentration of the precursors to completely fill the virus capsid.

Single molecule techniques provide detailed information not only about the structure but also about the key physical properties of nanoparticles. Specifically, atomic force microscopy (AFM), in contrast to EM, gives information about the 3D topographies of virus particles in air and liquid environments.[13] In addition, AFM provides information about a variety of physical properties, which may reveal crucial information about the internal structure of viruses.[14] The ultimate proof of functional magnetic particles would be detection of the magnetic signal from individual entities. Although magnetic force microscopy (MFM) has been suggested as a convenient tool for measuring the magnetism of single particles,[15−19] a correct interpretation of the MFM images of low-coercivity and low moment magnetic nanoparticles (MNPs) remains elusive.[20]

This paper focuses on the structural and magnetic characterization of individual cobalt-loaded CPMV eVLPs (Co-VLPs) and provides new insights on the metallic nanostructure formed within the eVLP.

MATERIALS AND METHODS

Empty and Loaded Virus Particles. Empty CPMV virus particles were propagated and isolated from plants, purified, and loaded with cobalt by published procedures.[9,10] The eVLPs were treated with chymotrypsin to enzymatically cleave off the C-terminal 24-amino acid peptide prior to loading to ensure homogeneity of the particles and so as to maximize internal loading.[21]

Procedures for the Adsorption of Particles on Surfaces. The virus particles were stored in a solution of phosphate-buffered saline (PBS) 100 mM, pH 7.0. To prepare AFM samples, 30 μL was placed in highly ordered pyrolytic graphite (HOPG), to provide a smooth surface for the AFM studies and left for 30 min for the particles to settle on the surface. Thereafter, the samples were washed with Milli-Q water and dried with argon for AFM and MFM characterization. For AFM measurements in liquid solutions, samples were washed in the same buffer (10 mM sodium phosphate buffer pH 7.2) in which the viruses were diluted in order to avoid the sample drying out and to remove the unattached particles.

To obtain a homogeneous dispersion of cobalt nanoparticles (CoNPs), 1 mg of carbon-coated cobalt nanoparticles (Sigma-Aldrich, CAS # 7440-48-4) were suspended in 1 mL of Milli-Q water containing sodium dodecyl sulfate (SDS, Sigma-Aldrich) 0.01%. These suspensions were sonicated for 2 h (frequency, 24 kHz; amplitude, 210 μm) on a UP400S Hielscher ultrasonic tip, Model H3-Tip3 (3 mm diameter). From the resulting colloidal suspension 40 μL were deposited by drop-casting on a mica surface functionalized with 3-aminopropyltriethoxysilane (APTS, Sigma-Aldrich). After 1 h, the samples were dried under argon, washed with Milli-Q water, and dried again under argon.

Magnetic Force Microscopy (MFM). The magnetic characterization was performed with a commercial MFM from Nanotec Electronica S.L. (Madrid, Spain). A magnetic probe attached to the end of a cantilever was used as the force sensor. Commercial nanosensors PPP-MFMR and budget sensors MFM (k = 1.5 N/m and f = 75 kHz) were used. Before each experiment, the probes were magnetized along their pyramid axis to ensure a maximum interaction between the tip and the sample. To measure a magnetic signal with MFM dynamic modes were employed (amplitude modulation in the case of ambient conditions, drive amplitude modulation at high vacuum).[21] The interaction between the magnetic moments of the tip and the sample, F_z, induces a change in the resonance frequency of the cantilever with the distance z. This frequency shift ($\Delta\omega$) can be correlated with the force gradient as is shown in eq 1:

$$\Delta\omega = \frac{\omega_0}{2k}\frac{\partial F_z}{\partial z} \quad (1)$$

where ω_0 is the resonance frequency and k is the force constant of the cantilever.

The isolation of electrostatic forces, which are simultaneously present to magnetic forces, is achieved with Kelvin probe force microscopy as explained elsewhere.[22] When very low magnetic signals are measured, the presence of other long-range interactions, like

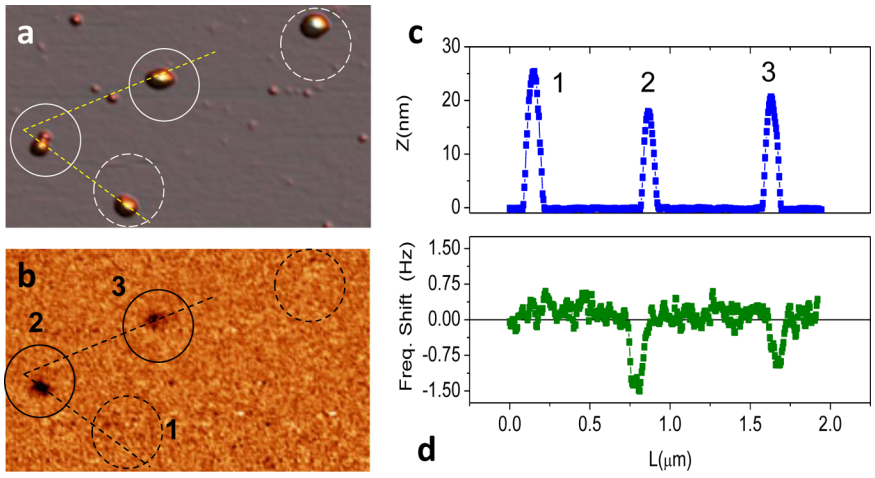

Figure 2. Magnetic characterization of commercial CoNPs particles. (a) Topography of CoNPs, (b) frequency shift caused by the tip−particle magnetic interaction, and (c, d) profiles of topography and magnetic interaction, respectively, along the corresponding lines 1-2-3. Images dimensions 1.9 × 1.4 μm.

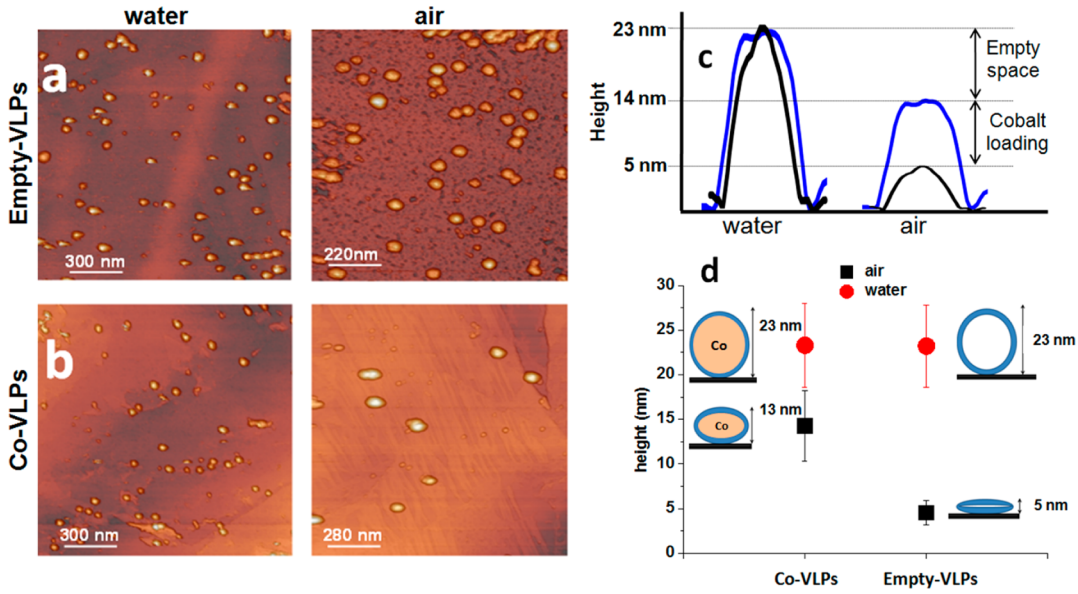

Figure 3. AFM images of desiccation effects on CPMV particles. (a) eVLPS on the surface in water (left) and air (right). (b) Co-VLPs on the surface, in water (left) and air (right). (c) Topographical profiles of single eVLPs and Co-VLPs, in black and blue, respectively. (d) Average height of eVLPs and Co-VLPs in air (black) and water (red). The numbers of eVLPs in water andair are 46 and 54, respectively. The numbers of Co-VLPs in water and air are 34 and 40, respectively. Error bars refer to the standard deviation. Insets depict cartoons of the role of the filling on the height of the particle.

electrostatic, can hide the magnetic information. We utilized HOPG (a conductor) to induce the charge migration and isolate the magnetic signal from the electrostatic one. In the case of commercial cobalt nanoparticles, the magnetic signal was large enough, so the combination of MFM + KPFM + HOPG was not needed.

Thermogravimetric Analysis (TGA). Experiments were conducted using a PerkinElmer Diamond TG/DTA Instrument between room temperature and 900 °C at a heating rate of 100 °C min^{-1} under an air flow of 200 mL min^{-1}. Zero grade air was supplied from BOC gases. The sample was loaded to a clean pan supported by a precision balance and the mass of the sample was monitored during the experiment. The purified Co-VLPs were either freeze-dried (−50 °C under vacuum and pressure) prior to TGA analysis or the Co-VLPs were loaded to the pan and the temperature raised to 100 °C and held at that temperature for 15 min to ensure the removal of all the moisture before continuing the experiment.

RESULTS

To determine the capability of MFM to detect the magnetism of the cobalt within a single Co-VLP, a control experiment was performed on a similar-sized commercial carbon-coated cobalt nanoparticle (CoNP) that possesses high magnetization values at room temperature (160 emu/g). CoNPs were immobilized on a mica surface. The CoNPs' size distribution was determined experimentally to be 19 ± 4 nm (average ± standard deviation, 50 particles), in agreement with the manufacturer's data. Figure 2a,b presents simultaneous topography and magnetic images of CoNPs, respectively, obtained at a retrace distance of 20 nm in air conditions.

In the case of protein shells, both empty and Co-filled virus particles (Co-VLPs) were explored by immobilizing them on HOPG and SiO_2 surfaces. Protein shells are severely affected by dehydration. In particular, virus structures are prone to collapse

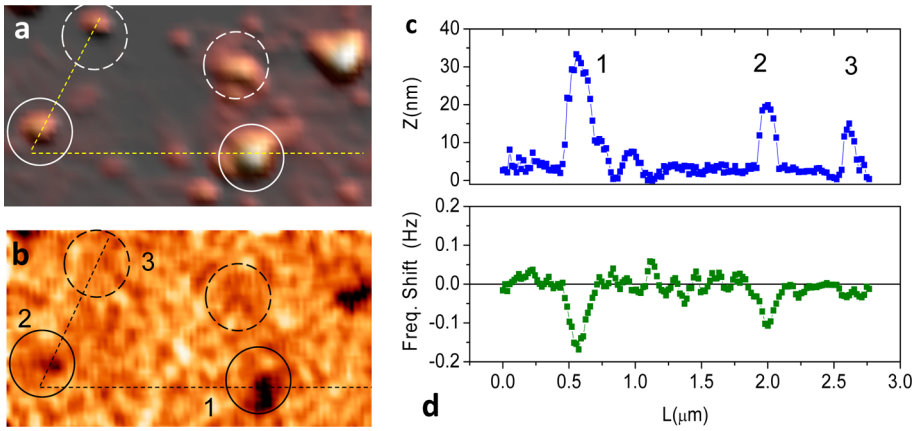

Figure 4. Magnetic characterization of Co-VLPs. (a) Topography of Co-VLPs, (b) frequency shift caused by the tip-particle magnetic interaction, and (c, d) profiles of topography and magnetic signal, respectively, along the corresponding lines 1-2-3. Images dimensions 1.9 × 1.4 μm.

wall-to-wall because of the capillary forces of water menisci during the last stages of desiccation processes.[13] This effect is modulated by the presence of the genetic material within wild-type particles, which prevents the wall-to-wall collapse. To unveil the effects of desiccation, AFM topographies for eVLPs and Co-VLPs adsorbed on HOPG were obtained in both water and air, as shown in Figure 3a,b, respectively. Figure 3c compares typical topographical profiles of viruses obtained in water (left) and air (right). The AFM data in water revealed that the height of eVLPs and Co-VLPs are similar between them and 4 nm below their nominal diameter,[23] as expected. Virus particles typically deform upon adsorption on surfaces because of their interaction with the surface.[14]

In addition, although desiccated Co-VLPs have a lower height than eVLPs in liquid, they have a greater height than dehydrated eVLPs. Indeed, a detailed statistical analysis (Figure 3d) indicates that eVLPs collapse wall-to-wall to 5 nm in height when desiccated, whereas Co-VLPs retain a height of about 14 nm. In the case of using SiO_2, and due to weak particle−surface interactions, both eVLPs and Co-VLPs show larger heights (less collapse), although still Co-VLPs are bigger than eVLPs (see the Supporting Information). Thus, the adsorption force of particles on HOPG is higher than when SiO_2 is used. As a consequence, eVLPs do not collapse wall-to-wall in SiO_2 and Co-VLPs' height is less sensitive to the amount of Co mass than when adsorbed on OPG. Hence, HOPG data was utilized for analysis.

In general, magnetic nanoparticles present a low magnetic moment at room temperature and heterogeneous electrostatic interactions with the tip,[20] impairing a direct interpretation of these experiments. MFM and Kelvin probe force microscopy (KPFM) experiments were performed in air and inside a high vacuum (HV) chamber, but magnetic signal was only observed when measuring in HV. The principal advantage of measuring in HV is the enhancement of the sensitivity due to the increment of the quality factor of the resonance[24] (we have increased the signal-to-noise ratio by a factor of ∼6). The topography and magnetic data obtained in HV for Co-VLPs are presented in Figure 4a,b. Figure 4c shows the corresponding profiles that allow an adequate identification of each particle with its magnetization.

We also utilized a bulk technique to estimate the nature of Co-VLPs to analyze the amount of cobalt inside viral particles. Thermogravimetric analysis (TGA) (Figure 5) determined for Co-VLPs that there was up to 55% mass loss from the starting

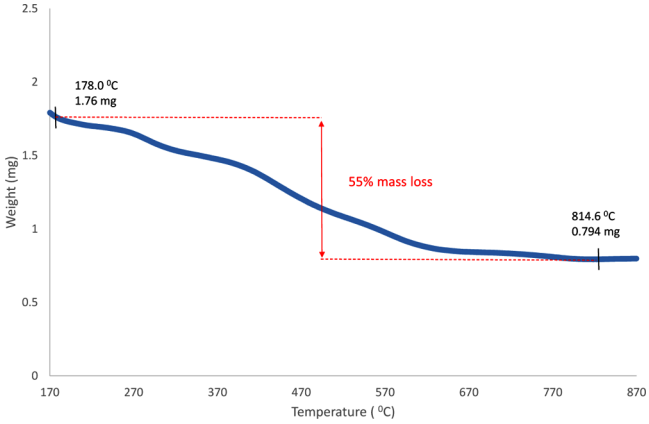

Figure 5. TGA curve of Co-VLPs lyophilized. The initial weight loss of samples observed around 100 °C is due to loss of moisture. By increasing the temperature, the weight residue declined at around 300 °C, probably due to the breakdown of side chain groups of amino acid residues of the virus capsid as well as the cleavage of peptide bonds.

material. If this mass loss is entirely attributed to the oxidative degradation of the protein shell, the remaining mass (45%) may be ascribed to the remaining metallic cobalt.

DISCUSSION

When CPMV eVLPs were incubated with cobalt ions, the cobalt cations interacted with the negatively charged amino acids within the virus capsid. The subsequent addition of the reducing agent ($NaBH_4$) generated solid metallic cobalt within the virus capsid. TEM suggested that the cavity of CPMV was completely filled with cobalt (Figure 1).[10] Our work aimed to investigate the quality of the VLPs from a practical point of view, i.e., how large is the magnetic interaction of a single Co-VLP? The magnitude of this magnetic signal would determine the capacity of these particles to be manipulated by magnetic fields. The magnetic interaction is related to the amount of Co inside the particle. Therefore, the primary objective was to evaluate the magnetic dipole of individual particles to establish a relationship with the amount of Co. The measurement of the magnetization of Co-VLPs at the single-particle level is attained with MFM.[25−27]

It is well-known that AFM can be used to detect different short-, medium-, and long-range interactions. However, the unknown contribution of every kind of force to the total force

measured hinders the amount of quantitative information that can be obtained from the measurements.[28] It should be noted that all the tip−sample interactions induce changes in the total force, i.e., they modify the cantilever state. In MFM, it is a usual procedure to separate the topography and the magnetic signal by scanning at a certain height such that the long-range tip−sample interactions dominate (typically 25−50 nm of retrace distance). An additional problem appears if several different long-range interactions are present between the tip and sample. In such a case, the best option is a combination of KPFM[22,29] and MFM to compensate the electrostatic contribution to the frequency shift signal.[28,30]

Most MFM measurements are based on the overall magnetic signal generated from the particles, regardless of possible variations between individual particles.[31] Besides, single particle experiments can determine the uniqueness of each entity and the uniformity or the lack of it between particles within the same sample. MFM characterization of individual Co-VLPs requires the selection of differential contrast experiments where the positive results should not be influenced by other variables such as topography, mechanical properties or electrostatic properties. However, magnetic measurements of the commercial CoNPs revealed such inhomogeneous magnetization. This can be observed in the corresponding profiles of two particles with similar size as shown in Figure 2c,d. Commercial CoNPs are passivized (coated) with a carbon layer that would avoid cobalt oxidation; any damage to this coating layer would result in cobalt oxidation, which will give CoNPs with variable magnetization uncorrelated with their size.

Because Co-VLPs and commercial CoNPs are of similar size, we expected to find similar magnetization values in the case of solid filling of Co-VLPs. However, the magnetic signal of Co-VLPs was very low when measured in ambient air. Therefore, high vacuum conditions were needed to increase the sensitivity of the magnetic measurements. Figure 4c reveals that the magnetization of Co-VLPs is not correlated with their size, thus showing that the amount of Co inside the viruses varies between particles. Furthermore, the Co-VLP signal is ∼8 times lower than that of the commercial CoNP, indicating that the amount of the magnetic Co inside virus particles is less than expected. Thus, we compared the Co-VLPs' signal with commercial Co-NPs of similar size, where it is known that Co spans the whole volume of the particle. We expected to find the Co-VLPs frequency shift comparable to the commercial particles. Because Co-VLPs show a 8-fold less frequency shift (∼0.2 Hz) than Co-NPs (∼1.5 Hz), it suggests that Co is not filling the available volume of the CPMV capsid. By attending to these data, we could roughly affirm that Co-VLPs have about 8 times less Co than commercial Co-NPs. Nevertheless, we pursued further AFM topography analyses in order to estimate the amount of Co inside the CPMV cavity. CPMV eVLPs and Co-VLPs show heights close to 23 nm in water (Figure 2), which coincides with the virus nominal size.[23] However, in air conditions, AFM topographies revealed a dramatic decrease of eVLP height to ∼5 nm on desiccation. In contrast, Co-VLPs height decreased to 14 nm in height after desiccation. In a similar case, it is known that DNA prevents partially the wall-to-wall collapse of bacteriophage ϕ29 virus cages under desiccation.[13] To what extent this collapse is prevented in Co-VLPs may signify the degree of filling of the virus cavity. The difference between heights observed for collapsed Co-VLP and eVLP (∼9 nm) establishes a top limit for the size of the cobalt cluster inside the viruses.

There are several possible explanations for the lack of material inside the Co-VLPs. First, cobalt could escape from the particles by the release of Co^{2+} cations upon oxidation, which would be apparent in the visible spectrum by the intense pink coloration of the hexaaquacobalt(II) complex. However, this phenomenon was not observed. Second, the AFM topographies are not compatible with the idea of solid nanoparticles filling the whole inner cavity of the virus. Our experiments inform about two facts: first, Co does not span the whole virus cavity, and second, its structure is not compact enough to support a dehydration process. There are two hypothetical structural motifs compatible with the experimental observations: (1) Cobalt might be structured in a thin layer carpeting the inner virus wall; (2) It could present a porous structure, corresponding to a noncontinuous metallic cluster like a sponge. These hypotheses are still consistent with the TEM images, which do not distinguish between solid nanoparticles occupying all the inner space of the virus and either a hollow Co shell or a sponge-like Co cluster (Figure 6). These hypotheses imply the presence of a lower amount of magnetic material, consistent with the low magnetic signal revealed by our MFM experiments.

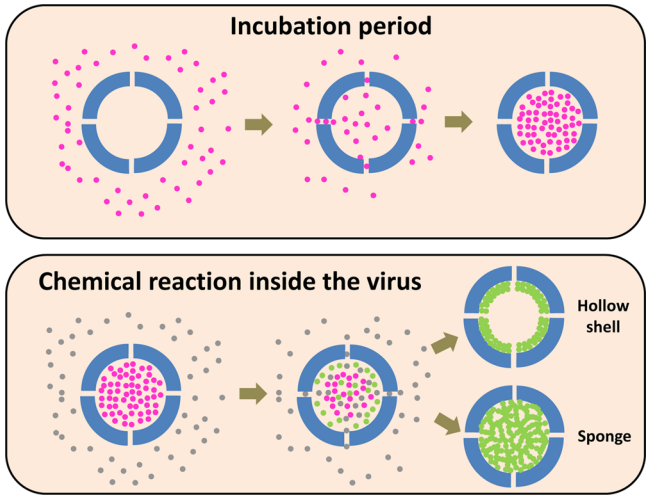

Figure 6. Schematic representation of the steps involved in the formation of cobalt within the virus capsid and of the chemical reaction for filling the capsid. The small pink spheres represent Co cations diffusing through the 12 pores on the virus capsid to the interior, and the incubation time allows interactions with the negatively charged amino acids present inside the capsid. The subsequent addition of the reducing agent $NaBH_4$ (black spheres) generates cobalt either as a hollow shell or a discontinuous cobalt cluster.

A rough approach to make a quantitative estimate of the cobalt inside one virus shell is to consider the virus as a spherical shell with an inner cavity of ∼12 nm in radius. By using the density of cobalt, the mass of metal filling a particle is 6.4×10^{-17} g (see the Supporting Information). Likewise, the mass of the proteinaceous shell reaches 5.6×10^{-18} g, thus indicating that for a 100% cobalt filled particle, 8% of the material is the protein shell (protein%), and 92% of the sample accounts for the loaded cobalt (cobalt%). Therefore, the ratio protein%/cobalt% = 0.086 for a solid filling. However, the TGA analysis (Figure 5) reveals that, for the Co-VLPs, this ratio increases to 55/45 = 1.22, suggesting that the virus particles are not fully loaded with cobalt. We can perform a similar

estimation with the AFM topographic data of Figure 3 (see the Supporting Information) to find a ratio of 55/45 = 1.22. Interestingly, both bulk and single-molecule topography techniques coalesce in estimating the amount of cobalt inside the Co-VLPs: the cobalt fills about 10% of the viral cavity volume (see the Supporting Information, supporting the absence of a solid filling.

Under the experimental conditions used, our findings may challenge the concept that the cavity of a virus can be completely filled by a nanoparticle grown in situ by a single chemical reaction inside the virus capsid. However, modification of the loading process might, in the future, lead to fuller loading by means of successive incubation-reduction cycles.

CONCLUSIONS

In our work, we have utilized a 2-fold approach to characterize individual cobalt structures grown within CPMV eVLPs, including both AFM topographies upon desiccation and magnetic force microscopy of individual particles. Both approaches suggest that the cobalt grown inside the virus shell can be described either as a hollow shell coating the inner wall of the virus or a porous sponge-like cobalt structure, revealing an incomplete filling of the virus cavity (10%), which we relate to the single incubation step of eVLPs in a solution containing a metal salt. Such noncompact metal distribution can be due to the fact that the amount of metal ions incorporated inside the virus during a single incubation period is never enough to fill all the empty space after chemical reduction. Consequently, an increase in the amount of magnetic material inside the capsid would require the implementation of multistep protocols including succesive incubation-metal-reduction cycles.

ASSOCIATED CONTENT

Supporting Information

Co-VLPs on SiO_2 and calculation of virus volume and weight ratios. This material is available free of charge via the Internet at http://pubs.acs.org.

AUTHOR INFORMATION

Corresponding Author

*P. J. de Pablo. E-mail: p.j.depablo@uam.es.

Present Addresses

[⊗]Faculty of Pharmacy, Yarmouk University, Irbid, Hashemite Kingdom of Jordan

[▽]Department of Chemistry, Indiana University, Bloomington, IN 47405, USA

Author Contributions

[¶]M. Jaafar and A. A. A. Aljabali contributed equally to this work.

Notes

The authors declare no competing financial interest.

ACKNOWLEDGMENTS

The authors acknowledge the MINECO of Spain (PIB2010US-00233, FIS3011-29493, CTQ2012-35513-C02 Consolider CSD2010-00024, CAM project No. S3009/MAT-1467) (P.J.P., M.J., I.B. and R.M.) This work was supported by BB/J004561/1 from the UK Biotechnology and Biological Sciences Research Council (BBSRC) and the John Innes Foundation (to D.J.E. and G.P.L.) and a BBSRC DTG (to A.A.A.A. and P.S.)

REFERENCES

(1) Douglas, T.; Young, M. Host-Guest Encapsulation of Materials by Assembled Virus Protein Cages. *Nature* **1998**, *393* (6681), 152–155.

(2) Douglas, T.; Strable, E.; Willits, D.; Aitouchen, A.; Libera, M.; Young, M. Protein Engineering of a Viral Cage for Constrained Nanomaterials Synthesis. *Adv. Mater. (Weinheim, Ger.)* **2002**, *14* (6), 415–418.

(3) Steinmetz, N. F.; Evans, D. J. Utilisation of Plant Viruses in Bionanotechnology. *Org. Biomol. Chem.* **2007**, *5* (18), 2891–2902.

(4) Evans, D. J. The Bionanoscience of Plant Viruses: Templates and Synthons for New Materials. *J. Mater. Chem.* **2008**, *18* (32), 3746–3754.

(5) Klem, M. T.; Young, M.; Douglas, T. Biomimetic Synthesis of Beta-TiO_2 inside a Viral Capsid. *J. Mater. Chem.* **2008**, *18* (32), 3821–3823.

(6) Wen, A. M.; Shukla, S.; Saxena, P.; Aljabali, A. A. A.; Yildiz, I.; Dey, S.; Mealy, J. E.; Yang, A. C.; Evans, D. J.; Lomonossoff, G. P.; Steinmetz, N. F. Interior Engineering of a Viral Nanoparticle and Its Tumor Homing Properties. *Biomacromolecules* **2012**, *13* (12), 3990–4001.

(7) Aljabali, A. A. A.; Shukla, S.; Lomonossoff, G. P.; Steinmetz, N. F.; Evans, D. J. CPMV-DOX Delivers. *Mol. Pharmaceutics* **2013**, *10* (1), 3–10.

(8) Saunders, K.; Sainsbury, F.; Lomonossoff, G. P. Efficient Generation of Cowpea Mosaic Virus Empty Virus-like Particles by the Proteolytic Processing of Precursors in Insect Cells and Plants. *Virology* **2009**, *393* (2), 329–337.

(9) Peyret, H.; Lomonossoff, G. P. The Peaq Vector Series: The Easy and Quick Way to Produce Recombinant Proteins in Plants. *Plant Mol. Biol.* **2013**, *83* (1–2), 51–58.

(10) Aljabali, A. A. A.; Sainsbury, F.; Lomonossoff, G. P.; Evans, D. J. Cowpea Mosaic Virus Unmodified Empty Viruslike Particles Loaded with Metal and Metal Oxide. *Small* **2010**, *6* (7), 818–821.

(11) Laurent, S.; Dutz, S.; Hafeli, U. O.; Mahmoudi, M. Magnetic Fluid Hyperthermia: Focus on Superparamagnetic Iron Oxide Nanoparticles. *Adv. Colloid Interface Sci.* **2011**, *166* (1–2), 8–23.

(12) Giustini, A. J.; Petryk, A. A.; Cassim, S. M.; Tate, J. A.; Baker, I.; Hoopes, P. J. Magnetic Nanoparticle Hyperthermia in Cancer Treatment. *Nano LIFE* **2010**, *1* (1n02).

(13) Carrasco, C.; Douas, M.; Miranda, R.; Castellanos, M.; Serena, P. A.; Carrascosa, J. L.; Mateu, M. G.; Marques, M. I.; de Pablo, P. J. The Capillarity of Nanometric Water Menisci Confined inside Closed-Geometry Viral Cages. *Proc. Natl. Acad. Sci. U. S. A.* **2009**, *106* (14), 5475–5480.

(14) Ortega-Esteban, A.; Pérez-Berná, A. J.; Menéndez-Conejero, R.; Flint, S. J.; San Martín, C.; de Pablo, P. J. Monitoring Dynamics of Human Adenovirus Disassembly Induced by Mechanical Fatigue. *Sci. Rep.* **2013**, *3*, 1434.

(15) Vergara, J.; Madurga, V.; Eames, P.; Dan Dahlberg, E. Magnetic Force Microscopy Observations of Co Nanoparticles Grown on Annealing Co_{10} Cu_{90} Melt Spun Ribbons. *J. Appl. Phys.* **2006**, *99* (5), 053910-1–053910-4.

(16) Diebel, C. E.; Proksch, R.; Green, C. R.; Neilson, P.; Walker, M. M. Magnetite Defines a Vertebrate Magnetoreceptor. *Nature* **2000**, *406* (6793), 299–302.

(17) Huang, X. L.; Bronstein, L. M.; Retrum, J.; Dufort, C.; Tsvetkova, I.; Aniagyei, S.; Stein, B.; Stucky, G.; McKenna, B.; Remmes, N.; Baxter, D.; Kao, C. C.; Dragnea, B. Self-Assembled Virus-like Particles with Magnetic Cores. *Nano Lett.* **2007**, *7* (8), 2407–2416.

(18) Moskalenko, A. V.; Yarova, P. L.; Gordeev, S. N.; Smirnov, S. V. Single Protein Molecule Mapping with Magnetic Atomic Force Microscopy. *Biophys. J.* **2010**, *98* (3), 478–487.

(19) Schreiber, S.; Savla, M.; Pelekhov, D. V.; Iscru, D. F.; Selcu, C.; Hammel, P. C.; Agarwal, G. Magnetic Force Microscopy of Superparamagnetic Nanoparticles. *Small* **2008**, *4* (2), 270–278.

(20) Neves, C. S.; Quaresma, P.; Baptista, P. V.; Carvalho, P. A.; Araujo, J. P.; Pereira, E.; Eaton, P. New Insights into the Use of

Magnetic Force Microscopy to Discriminate between Magnetic and Nonmagnetic Nanoparticles. *Nanotechnology* **2010**, *21* (30), 305706.
(21) Sainsbury, F.; Saunders, K.; Aljabali, A. A. A.; Evans, D. J.; Lomonossoff, G. P. Peptide-Controlled Access to the Interior Surface of Empty Virus Nanoparticles. *ChemBioChem* **2011**, *12* (16), 2435−2440.
(22) Jaafar, M.; Iglesias-Freire, O.; Serrano-Ramon, L.; Ibarra, M. R.; de Teresa, J. M.; Asenjo, A. Distinguishing Magnetic and Electrostatic Interactions by a Kelvin Probe Force Microscopy-Magnetic Force Microscopy Combination. *Beilstein J. Nanotechnol.* **2011**, *2*, 552−560.
(23) Lin, T. W.; Chen, Z. G.; Usha, R.; Stauffacher, C. V.; Dai, J. B.; Schmidt, T.; Johnson, J. E. The Refined Crystal Structure of Cowpea Mosaic Virus at 2.8 Angstrom Resolution. *Virology* **1999**, *265* (1), 20−34.
(24) Grutter, P.; Liu, Y.; LeBlanc, P.; Durig, U. Magnetic Dissipation Force Microscopy. *Appl. Phys. Lett.* **1997**, *71* (2), 279−281.
(25) Martin, Y.; Williams, C. C.; Wickramasinghe, H. K. Atomic Force Microscope Force Mapping and Profiling on a Sub 100-Å Scale. *J. Appl. Phys.* **1987**, *61* (10), 4723−4729.
(26) Saenz, J. J.; Garcia, N.; Grutter, P.; Meyer, E.; Heinzelmann, H.; Wiesendanger, R.; Rosenthaler, L.; Hidber, H. R.; Gunterodt, H. J. Observation of Magnetic Forces by the Atomic Force Microscope. *J. Appl. Phys.* **1987**, *62* (10), 4293−4295.
(27) Schwarz, A.; Wiesendanger, R. Magnetic Sensitive Force Microscopy. *Nano Today* **2008**, *3* (1−2), 28−39.
(28) Glatzel, T.; Sadewasser, S.; Lux-Steiner, M. C. Amplitude or Frequency Modulation-Detection in Kelvin Probe Force Microscopy. *Appl. Surf. Sci.* **2003**, *210* (1−2), 84−89.
(29) Palacios-Lidon, E.; Colchero, J. Quantitative Analysis of Tip-Sample Interaction in Non-Contact Scanning Force Spectroscopy. *Nanotechnology* **2006**, *17* (21), 5491−5500.
(30) Martinez-Martin, D.; Jaafar, M.; Perez, R.; Gomez-Herrero, J.; Asenjo, A. Upper Bound for the Magnetic Force Gradient in Graphite. *Phys. Rev. Lett.* **2010**, *105* (25), 257203.
(31) Puntes, V. F.; Gorostiza, P.; Aruguete, D. M.; Bastus, N. G.; Alivisatos, A. P. Collective Behaviour in Two-Dimensional Cobalt Nanoparticle Assemblies Observed by Magnetic Force Microscopy. *Nat. Mater.* **2004**, *3* (4), 263−268.